Journal of Geophysical Research: Solid Earth

Supporting Information for

Similarities and differences in the rupture processes of the 1952 and 2003 Tokachi-oki earthquakes

Hiroaki Kobayashi[1*], Kazuki Koketsu[1], Hiroe Miyake[1], and Hiroo Kanamori[2]

[1]Earthquake Research Institute, University of Tokyo, Tokyo, Japan

[2]Seismological Laboratory, California Institute of Technology, Pasadena, California, U.S.A.

[*]Present address: Kobori Research Complex Inc., Tokyo, Japan

Contents of this file

Introduction

In this supporting information, the weighting scheme and detailed results in the inversion analyses, comparisons of magnitudes, waveform comparisons of two M7 earthquake pairs, station information, instrument constants of the analog seismographs, and velocity structure models for calculating the teleseismic and geodetic Green's functions are provided. Text S1 describes the method of weighting in the inversion analyses. Text S2 demonstrates the details of the comparisons of m_B, the body wave magnitude, and M_S, the surface wave magnitude, between the 1952 and 2003 earthquakes. Figure S1 shows the slip distribution obtained with the 2003-S dataset by minimizing the Akaike's Bayesian information criterion. Figures S2 and S3 show the data fits of the inversion analyses using the 2003-S and 1952-S datasets, respectively. Figure S4 shows the moment rate functions of the three inversion analyses. Figure S5 shows the waveforms from the near trench slip in the 2003-S model. Figure S6 compares m_B and M_S for the 1952 and 2003 earthquakes. Figure S7 shows waveform comparisons for the two pairs of M7 earthquakes in the Akkeshi-oki region. Tables S1 and S2 provide the instrument constants of the analog seismographs. Table S3 lists the information concerning the strong motion station pairs. Tables S4–S6 provide the one-dimensional (1D) velocity structure models used to calculate the teleseismic and geodetic Green's functions.

Text S1.

The objective function S minimized in our source inversion is,

$$S = \sum_{ijk} w_{j,k}^{f}\left\{F_{j,k}^{O}(t_i) - F_{j,k}(t_i)\right\}^2 + w^g \sum_{jk}\left\{U_{j,k}^{O} - U_{j,k}\right\}^2 + \beta^2\left\{\sum_{mnl}\nabla^2 X_{mnl} + \sum_{mnl}\nabla^2 Y_{mnl}\right\}, \quad (1)$$

where $F_{j,k}^{O}(t_i)$ and $F_{j,k}(t_i)$ are the observed and synthetic waveforms of the k-th component at the j-th station at time t_i, respectively, $U_{j,k}^{O}$ and $U_{j,k}$ are the observed and synthetic static displacements, respectively, $w_{j,k}^{f}$ is the weight for the waveform of the k-th component at the j-th station. w^g is the weight for a static displacement, β is the weight for the spatial and temporal smoothness constraints, and X_{mnl} and Y_{mnl} are the slip amounts of the l-th time window on the mn-th subfault in the X- and Y- directions, respectively. ∇^2 is the discrete Laplacian operator defined as

$$\begin{aligned}\nabla^2 X_{mnl} = {} & X_{m+1,n,l} + X_{m-1,n,l} - 2X_{m,n,l} \\ & + \frac{\Delta x^2}{\Delta y^2}\left(X_{m,n-1,l} + X_{m,n-1,l} - 2X_{m,n,l}\right) \\ & + \frac{\Delta x^2}{\tau^2 V_{\mathrm{r}}^2}\left(X_{m,n,l+1} + X_{m,n,l-1} - 2X_{m,n,l}\right),\end{aligned} \quad (2)$$

where Δx and Δy are the length and width of the subfault, respectively, τ is the width of the basis time function, and V_{r} is the rupture front velocity. We set $w_{j,k}^{f}$ such that

$$w_{j,k}^{f} = \frac{c}{\sum_l F_{j,k}^{O}(t_l)^2}, \quad (3)$$

where c is a constant, and $w_{j,k}^{g}$ such that

$$w^g = c\frac{2n_h + n_v}{\sum_{jk} {U_{j,k}^{O}}^2}, \quad (4)$$

where n_h and n_v are the number of horizontal and vertical components, respectively. β was determined by minimizing the Akaike's Bayesian information criterion (ABIC) (Akaike, 1980) in the 2003-L dataset. However, in the 2003 S dataset, we did not use the ABIC because an unreasonable slip distribution was obtained when minimizing the ABIC (Figure S1). This is likely due to the small amount of data in the 2003-S dataset. Instead, we determined β such that the seismic moment for the main rupture area in the Tokachi-oki region was nearly the same as that determined with the 2003-L dataset. We used the same β values for the 1952-S and 2003-S datasets.

Text S2.

The earthquake magnitude scale is a somewhat primitive parameter; however, it is useful for comparing old and recent earthquakes with modern seismic data. In fact, for old earthquakes with limited instrumental data, it is the only quantitative instrumental parameter available for the earthquake size. In particular, the magnitude values computed by Gutenberg for Seismicity of the Earth (Gutenberg and Richter, 1954) incorporate amplitude data reported by many observatories and the instrument characteristics are believed to be more reliable than those compiled later.

The original handwritten notes by Gutenberg, generally referred to as the "Gutenberg Notepad" (Goodstein et al., 1980), are archived at the California Institute of Technology. The result for the 1952 Tokachi-oki earthquake is on page 335 of Pad #106.

The body-wave magnitude m_B was developed by Gutenberg and Richter (1942, 1955) and is the only magnitude scale that can be used for both shallow and deep earthquakes in the world. Kanamori and Ross (2019) followed the original Gutenberg-Richter's method as closely as possible and computed m_B for events larger than M_W 6 for the period from 1988 to 2018. Figure S6a shows a comparison of the 1952 and 2003 earthquakes. Gutenberg and Richter (1954) (also Abe, 1981) calculated $m_B = 8$ for the 1952 event, and m_B (median) for the 2003 event listed in Kanamori and Ross (2019) is 7.69 with a standard deviation of 0.26 (stations DPC and HNR were rejected). Even though, as noted in Kanamori and Ross (2019), there are some differences in the methods (e.g., types of instruments, phases, and periods), the difference of approximately 0.3 between the 1952 and 2003 earthquakes is qualitatively consistent with the amplitude difference.

Comparisons of M_S between old and recent events are not straightforward. The M_S value in the notepad was computed from the horizontal component of the surface waves using the formula given in Gutenberg (1945) with some station corrections that were not well documented. For recent events, we use a method similar to that used by the National Earthquake Information Center of the U.S. Geological Survey. In this method, only vertical component records are used with the formula given by Vanek et al. (1962). At face value, the use of different formula and components suggests that the modern M_S is larger than the old M_S by approximately 0.18. However, there are other complications, as discussed in Geller and Kanamori (1977), and the difference appears to be insignificant, as demonstrated by Lienkaemper (1984). Therefore, we assume that there is no bias between the old and modern M_S values. In fact, a more serious problem is the path effect which often results in an M_S difference of 1.5. The advantage of using the original data listed in the Gutenberg Notepad, rather than the average values of M_S published in various catalogs, is that we can compare the modern and old M_S values for the same source-path combinations, therefore minimizing the path effects. Accordingly, the difference in M_S is more reliable than the absolute value.

Figure S6b compares the M_S values for the 1952 and 2003 earthquakes determined using this method. For the 1952 earthquake, Abe (1981) calculated M_S = 8.3, and for the 2003 earthquake, we obtained M_S (median) = 8.17 with a standard deviation of 0.29. Given all the uncertainties involved in the M_S determinations, a reasonable conclusion is that the 1952 and the 2003 earthquakes have approximately the same M_S. As shown in Figure S4, the moment rate functions for the 1952 and 2003 earthquakes suggest that M_W is slightly larger for the 1952 earthquake than for the 2003 earthquake, but that the moment rate function of the 1952 earthquake exhibits two peaks, and the spectral amplitude approximately at about 20 s can be complex. Therefore, a comparable M_S for the 1952 and 2003 earthquakes appears reasonable.

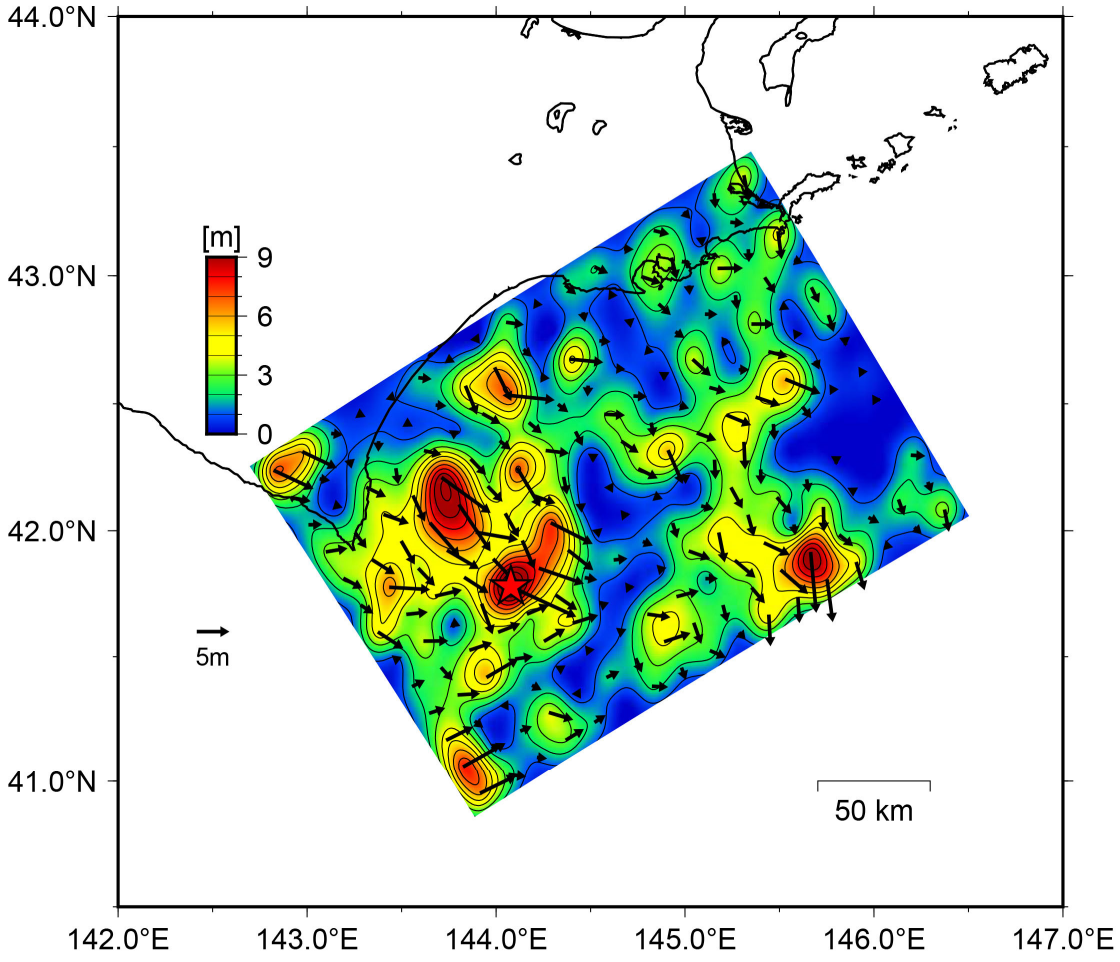

Figure S1. Slip distribution obtained with the 2003-S dataset by minimizing the ABIC.

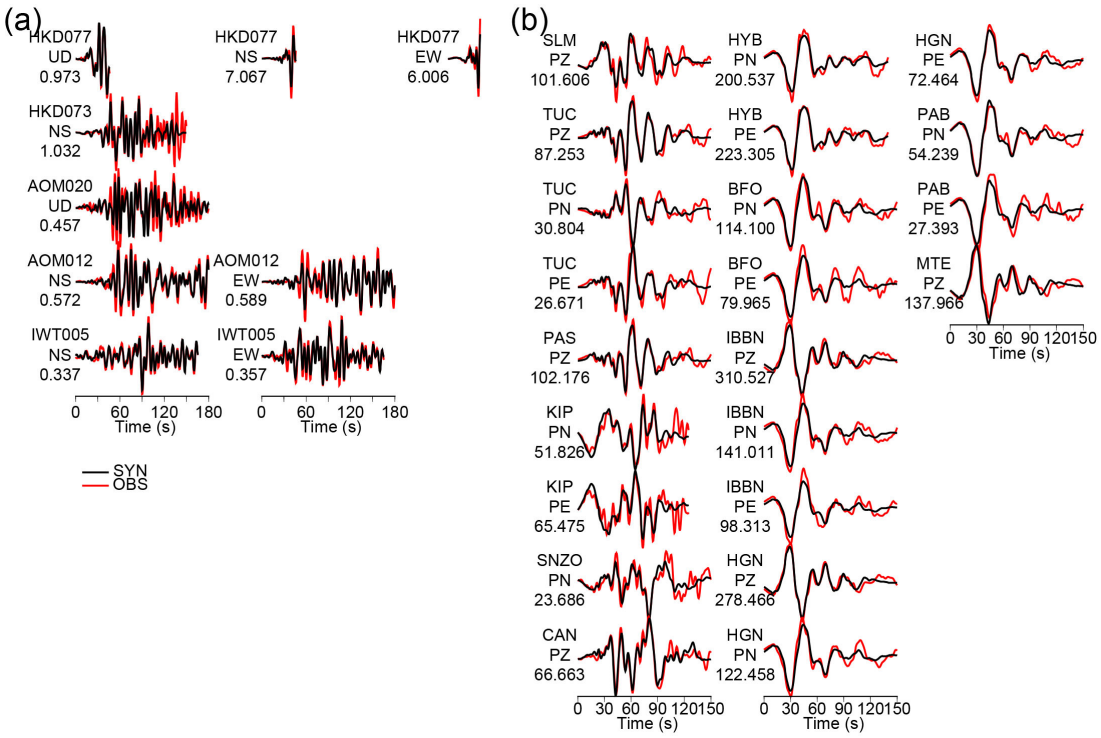

Figure S2. (a) Strong motion, and (b) teleseismic data fits of the 2003-S dataset. The observed and synthetic data are shown by the red and black lines, respectively. The station names, components, and maximum amplitude (cm for strong motion and μm for teleseismic) of the observed waveforms are shown to the left of each waveform.

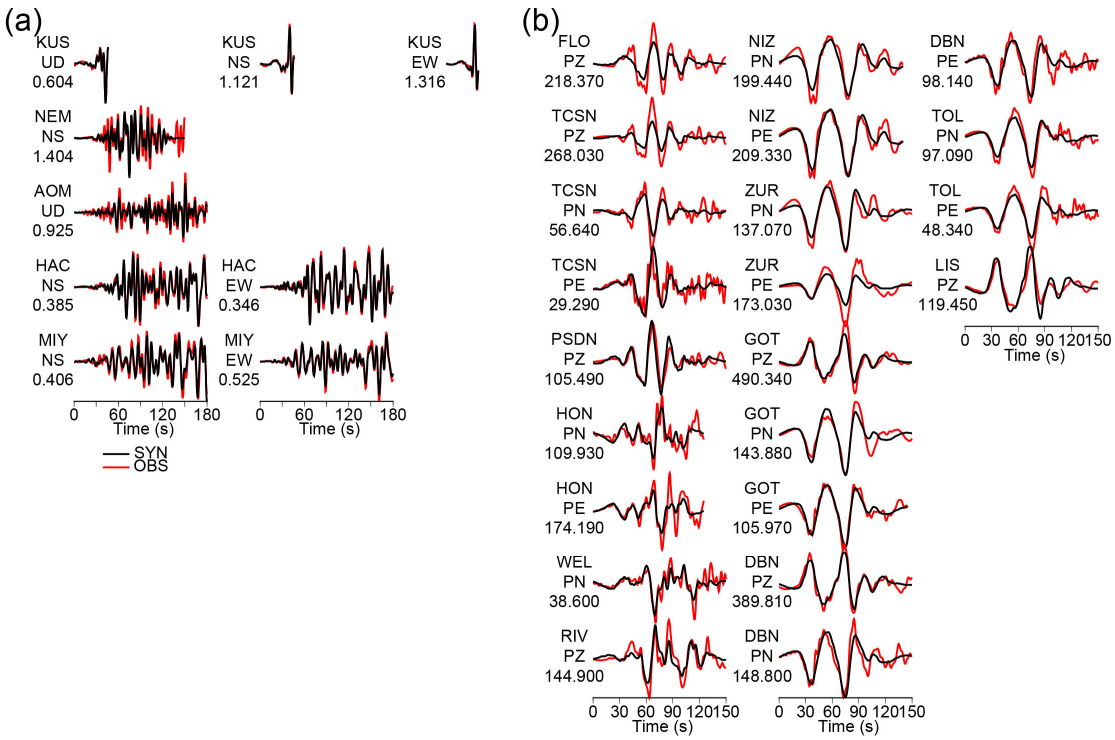

Figure S3. (a) Strong motion, and (b) teleseismic data fits of the 1952-S dataset. The observed and synthetic data are shown by the red and black lines, respectively. The station names, components, and maximum amplitude of the observed waveforms (cm for strong motion and μm for teleseismic) are shown to the left of each waveform.

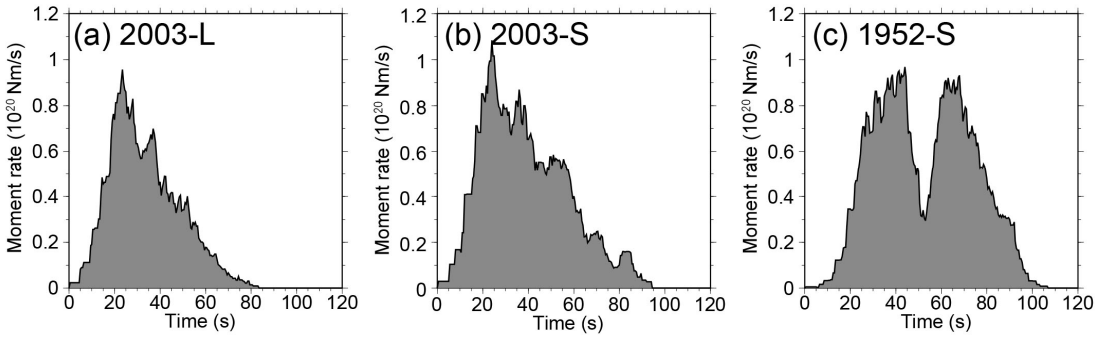

Figure S4. Moment rate functions determined using the (a) 2003-L, (b) 2003-S, and (c) 1952-S datasets.

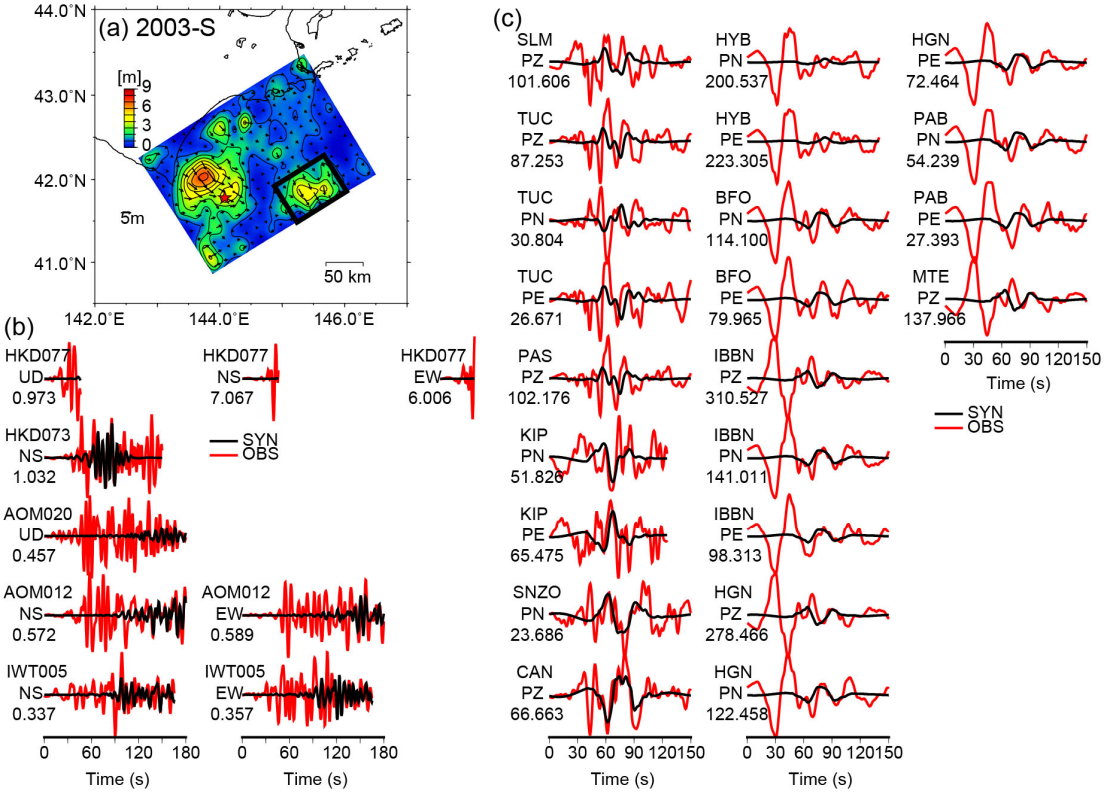

Figure S5. Synthetic waveforms from the near trench slip in the 2003-S model (a) Slip distribution of the 2003-S model. The thick black rectangle indicates the region selected for the calculation of the synthetic waveforms. Synthetic (b) strong motion and (c) teleseismic waveforms are shown by the black lines. The observed waveforms are shown by the red lines. The station names, components, and maximum amplitude of the observed waveforms (cm for strong motion and μm for teleseismic) are shown to the left of each waveform.

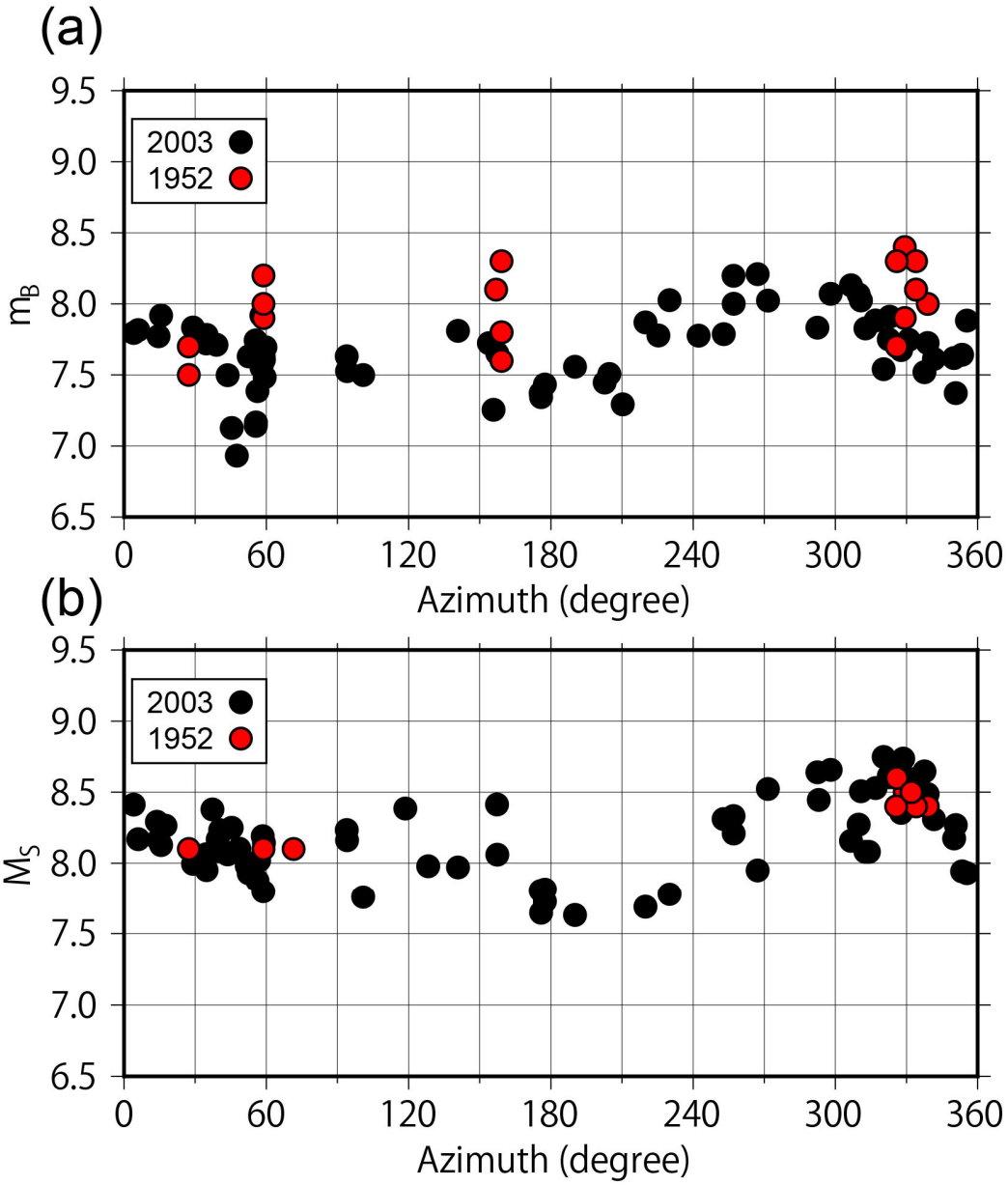

Figure S6. Comparisons of the azimuthal distributions of (a) m_B and (b) M_S for the 1952 and 2003 Tokachi-oki earthquakes. The black and red circles indicate the values for the 2003 and 1952 earthquakes, respectively.

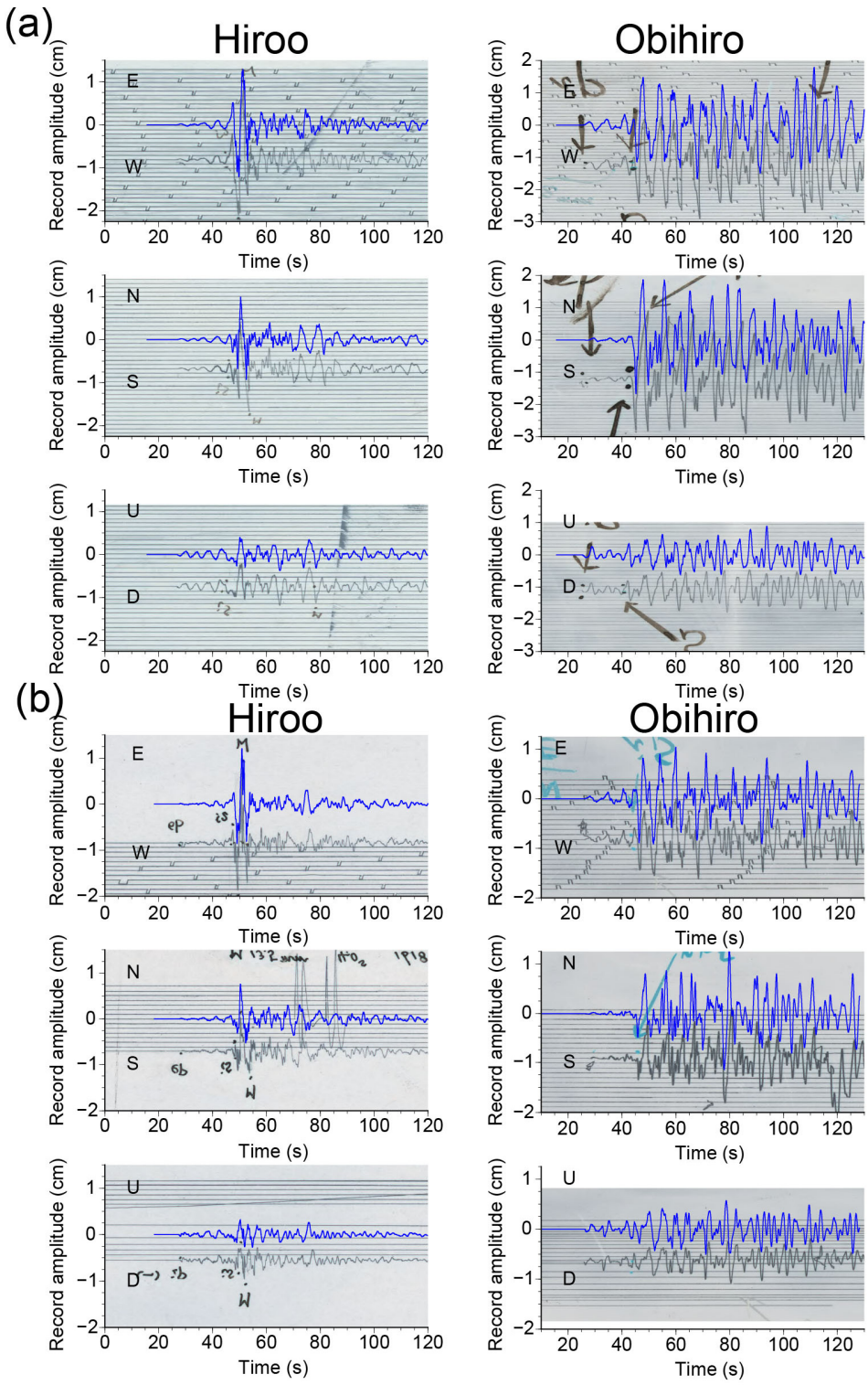

Figure S7. Comparisons of the observed waveforms at the Hiroo and Obihiro stations (a) between the 28 November 2004, M_{JMA} 7.1 and 11 August 1961, M_{JMA} 7.2 earthquakes and (b) between the 06 December 2004, M_{JMA} 6.9 and 15 November 1961, M_{JMA} 6.9

earthquakes. For each waveform pair, the 2004 waveform is corrected to simulate the 1961 instrument response. The blue lines and the background images show the observed waveforms of the 2004 and 1961 earthquakes, respectively.

Table S1. Instrument constants for the seismographs at the teleseismic stations.

Station	Seismograph	Comp.	V	T_0	ε	V_m	T_l	T_g	Source
Florissant (FLO)	Galitzin	UD				694	12	11.7	Alvarado and Beck (2006)
Tucson (TCSN)	Benioff	UD			h_l = 0.8 h_g = 1.0	3000	1	77	Microfilm V_m is from Alvarado and Beck (2006)
	Wood-Anderson	NS	466	8	77				Microfilm
	Wood-Anderson	EW	457	8	107				Microfilm
Pasadena (PSDN)	Benioff	UD				3000	1	90	Microfilm
Honolulu (HON)	Milne-Shaw	NS	124	12	20				Charlier and Van Gils (1953)
	Milne-Shaw	EW	142	12	20				Charlier and Van Gils (1953)
Wellington (WEL)	Milne-Shaw	NS	250	12	20				Scanned image
Riverview (RIV)	Galitzin	UD				460	10.8	10.9	Station bulletin
Nizamia (NIZ)	Milne-Shaw	NS	249	12	20				Station bulletin
Nizamia (NIZ)	Milne-Shaw	EW	249	12	20				Station bulletin
Zurich (ZUR)	Mainka	NS	140	7	3				Charlier and Van Gils (1953)
	Mainka	EW	140	7	3				Charlier and Van Gils (1953)
Gottingen (GOT)	Wiechert	UD	177	5.1	3.9				Estabrook et al. (1994)
	Wiechert	NS	143	10.1	2.9				Station bulletin
	Wiechert	EW	140	13	4.1				Estabrook et al. (1994)
De Bilt (DBN)	Galitzin	UD				740	12	12	Charlier and Van Gils (1953)
	Galitzin	NS				310	25	25	Charlier and Van Gils (1953)
	Galitzin	EW				310	25	25	Charlier and Van Gils (1953)
Toledo (TOL)	Wiechert	NS	540	11	4.2				Station bulletin
	Wiechert	EW	530	11	4.1				Station bulletin
Lisbon (LIS)	Wiechert	UD	205	4.9	2.67				Station bulletin

Comp.: component (NS: north–south, EW: east–west, UD: up–down); V: magnification; T_0: natural period in s; ε: damping ratio; V_m: peak magnification; T_l: natural period of the pendulum in s; T_g: natural period of the galvanometer in s; h_l: damping constant of the pendulum; and h_g: damping constant of the galvanometer. We assumed $h_g = h_l = 1.0$ except for the Benioff seismograph in Tucson.

Table S2. Instrument constants for the seismographs of the near field stations.

Station	Seismograph	Comp.	V	T_0	ε	Source
Nemuro (NEM)	JMA type 50	NS	1	6	8	Hamamatsu (1966)
	Wiechert	NS	80	5	6	Hamamatsu (1966)
Kushiro (KUS)	JMA type 51	NS	1	6.2	13.5	Scanned image
	JMA type 51	EW	1	6.2	10.5	Scanned image
	JMA type 51	UD	1	6.0	5.4	Scanned image
	CMO portable	NS	40	4.0	7.7	CMO (1953)
	CMO portable	EW	40	4.1	6.7	CMO (1953)
Aomori (AOM)	JMA type 50	UD	1	5.0	8.0	CMO (1953)
	Wiechert	UD	83	3.3	5.8	CMO (1953)
Hachinohe (HAC)	JMA type 51	NS	1	6.0	8	CMO (1953)
	JMA type 51	EW	1	6.0	8	CMO (1953)
	Wiechert	NS	90	4.6	4.6	CMO (1953)
	Wiechert	EW	89	4.8	5.6	CMO (1953)
Miyako (MIY)	JMA type 51	NS	1	6.0	8.0	CMO (1953)
	JMA type 51	EW	1	6.0	8.0	CMO (1953)
	Wiechert	NS	96	5.2	6.4	CMO (1953)
	Wiechert	EW	94	5.0	5.6	CMO (1953)
Hiroo	JMA type 52B	NS	1	5.8	8	Sapporo Regional Headquarters and Obihiro Meteorological Station (1962)
	JMA type 52B	EW	1	6.0	8	
	JMA type 52B	UD	1	5.3	7	
Obihiro	JMA type 52	NS	1	5.1	8	
	JMA type 52	EW	1	5.1	7	
	JMA type 52	UD	1	4.7	6	

Comp.: component (NS: north–south, EW: east–west, UD: up–down); V: magnification; T_0: natural period in s; and ε: damping ratio.

Table S3. Information concerning the strong motion station pairs.

2003			1952		
Station	Lat. (°)	Lon. (°)	Station	Lat. (°)	Lon. (°)
HKD077	42.9845	144.3824	KUS	42.9809	144.3910
HKD073	43.3327	145.6003	NEM	43.3309	145.5826
AOM020	40.8193	140.7501	AOM	40.8527	140.6965
AOM012	40.5138	141.4805	HAC	40.5277	141.5214
IWT005	39.6472	141.9464	MIY	39.6478	141.9647

World Geodetic System coordinates are used.

Table S4. 1D near-source velocity structure model for the calculation of the teleseismic Green's functions.

Thickness (km)	V_p (km/s)	V_s (km/s)	ρ (10^3 kg/m^3)
1.0	1.5	0.0	1.02
0.5	2.0	0.6	2.00
0.75	2.4	1.0	2.15
2.5	3.0	1.5	2.25
0.75	3.5	2.0	2.35
7.5	5.8	3.4	2.70
12.0	6.4	3.8	2.8
∞	7.5	4.5	3.20

Table S5. 1D near-receiver velocity structure model for the calculation of the teleseismic Green's functions.

Thickness (km)	V_p (km/s)	V_s (km/s)	ρ (10^3 kg/m^3)
15.0	5.57	3.36	2.65
18.0	6.50	3.74	2.87
∞	8.10	4.68	3.30

Table S6. 1D velocity structure model for the calculation of the geodetic Green's functions.

Thickness (km)	V_p (km/s)	V_s (km/s)	ρ (10^3 kg/m^3)	Q_p	Q_s
5.5	5.5	3.2	2.65	680	400
7.5	5.8	3.4	2.7	680	400
12.0	6.4	3.8	2.8	680	400
∞	7.5	4.5	3.2	850	500